12. Buser, O., Two years' experience of operational avalanche forecasting using nearest neighbours method. *Ann. Glaciol.*, 1989, **13**, 31–34.
13. Carter, M. M. and Elsner, J. B., A statistical method forecasting rain over Puerto Rico. *Weather Forecast.*, 515–525.
14. Fukunaga, K. and Hostetler, Optimization of *k*-nearest neighbour density estimate. *IEEE Trans. Inf. Theor.*, 1973.
15. Thomas, J. H., Xufeng, N. and James, E. B., A space–time model for seasonal hurricane prediction. *Int. J. Climatol.*, 2002, **22**, 451–465.
16. Pirmin, K. and David, W. C., Cluster-analysis classification of winter wind patterns in the Grand Canyon region. *J. Appl. Meteorol.*, 1999, 1131–1147.
17. Mohanty, U. C. and Dimri, A. P., Location-specific prediction of the probability of occurrence and quantity of precipitation over western Himalaya. *Weather Forecast.*, 2004, **19**, 36–49.
18. Wilks, D. S., *Statistical Methods in Atmospheric Sciences*, Academic Press, New York, 1995.

ACKNOWLEDGEMENTS. We thank Dr R. N Sarwade, Director, Snow and Avalanche Study Establishment (SASE), Chandigarh for encouragement and scientists and technical assistants of Avalanche Forecasting Group, SASE who collected data under harsh climatic conditions in remote snow-bound areas.

Received 13 August 2004; revised accepted 7 January 2005

Synthetic accelerograms for two Himalayan earthquakes using convolution

V. N. Singh[1] and Abha Mittal[2,*]

[1]Department of Earth Sciences, Indian Institute of Technology, Roorkee 247 667, India
[2]Central Building Research Institute, Roorkee 247 667, India

In the present communication, computation of synthetic accelerograms is based on convolution. The spectrum of ground motion expected at a recording site is first computed from a knowledge of source parameters and medium properties. This spectrum is then inverse Fourier transformed to yield the desired synthetic accelerogram. This method has been successfully used by Boore, and has been further extended in the present communication. The suitability of the method is demonstrated successfully by modelling the accelerograms for two Himalayan earthquakes namely, the 1991 Uttarkashi earthquake and the 1999 Chamoli earthquake and compared with the observed accelerograms.

EARTHQUAKE-resistant design of engineering structures is one of the most important methods of mitigating risk of damage from future earthquakes. Such designs are based on the specification of ground motion which can be expected in the event of an earthquake. However, for earthquake-resistant design of some important structures like dams and nuclear power plants, located in seismically active areas, it is desirable to have a reliable site-specific design accelerogram. Available records of strong ground motion, after suitable modifications, have been used in the past for detailed dynamic analysis of engineering structures. However, synthetic accelerograms are now increasingly being used in earthquake engineering. A knowledge of regional and local seismicity and seismotectonics, a suitable earth model and source characteristics of the design earthquake are required for this purpose.

There have been some recent attempts on new approaches to synthesize strong ground motions and to obtain source parameters[1–12].

Khattri *et al.*[13] and Yu *et al.*[11] carried out synthesis of strong motion for the Uttarkashi earthquake. Khattri *et al.*[13] carried out forward modelling using the isochrone method and inverted the observed accelerograms by recursive stochastic inverse algorithm to obtain the earthquake source slip function. Yu *et al.*[11] generated synthetics using the composite source model and synthetic Green's function. Solution of the forward problem carried out by Yu *et al.*[11] has taken into account the velocity structure in the Uttarkashi area and its Q-structure. The method of generating synthetics depends on the knowledge of many input parameters like velocity and Q-structure of the layered earth model. Kumar *et al.*[12] used semi-empirical method for calculating synthetic accelerograms. They divided the fault plane into sub-faults and generated envelop waveform, instead of actual time history, corresponding to each element of the fault plane.

In the present communication, an improved method of generating synthetic accelerograms has been presented and discussed. Generation of synthetic accelerograms in the near field is based on a dislocation moving over a fault plane. The computed ground motions have to take into account the nature of rupture propagation over the fault plane, radiation pattern effects, presence of free surface layering in the earth between the source and free surface and effect of finite moving source. The slip on the causative fault is specified in terms of shape, rise time and amplitude of the source time function. In addition, velocity of rupture propagation and final area over which slip occurs are also specified.

Let $y(t)$ represent the recorded seismogram at a point on the surface of a layered half space produced by a point shear dislocation. This can be written as:

$$y(t) = C*s(t)*a(t)*d(t)*i(t), \quad (1)$$

where C is a scalar, $s(t)$ is the source time function, $a(t)$ represents the impulse response of the layered medium between source and receiver, $d(t)$ accounts for frequency-dependent attenuation and $i(t)$ is the impulse response of the seismograph. In frequency domain, eq. (1) can be written as:

$$Y(\omega) = CS(\omega)A(\omega)D(\omega)I(\omega), \quad (2)$$

*For correspondence. (e-mail: abham2003@yahoo.com)

where each function of angular frequency ω represents the Fourier transform of the corresponding time function. All these functions are complex in ω.

Scalar C used in the synthesis is given by

$$C = M_o R_p F_s / 4\pi\rho c^3 r, \quad (3)$$

where M_o is the seismic moment which itself is the product of fault area, average dislocation and rigidity of the medium in which the fault is embedded[14]. R_p is the radiation pattern and F_s represents the effect of the presence of free surface, i.e. the factor by which ground motions are amplified by the presence of free surface[15]. The term ρ is density of the source region, c represents the P or S-wave velocity (α or β) and r is the source-to-receiver distance, i.e. hypocentral distance.

$S(\omega)$ represents the source spectral function. The function $A(\omega)$ accounts for the effect of the intervening medium between the source and receiver. It can be expressed as a frequency-dependent transfer function that results from wave propagation in a stack of layers with a strong impedance contrast at the base of the stack. Thus, as seismic waves approach the earth's surface they are amplified by gradual decrease in seismic impedance. In the case of a homogeneous elastic half space, the amplification factor $A(\omega)$ can be taken as unity.

Diminution function $D(\omega)$ accounts for the frequency-dependent attenuation due to the nature of the medium along the path followed by the seismic waves. The amplitude of the seismic waves from an earthquake source decreases with increasing distance because of geometrical spreading, energy partitioning at layer boundaries, diffraction, scattering and frequency-dependent attenuation resulting from the absorption and conversion of seismic energy into heat.

The attenuation is expressed by quality factor Q. The attenuation coefficient a is given by

$$a = \frac{\omega}{2CQ}. \quad (4)$$

So attenuation for a given wave type (P or S) is defined as the inverse of Q. Q has been found to be a function of frequency. A form of Q that fits a number of observations is given by[16]:

$$Q = 29.4 \frac{\left[1 + \frac{\omega}{0.6\pi}\right]^{2.9}}{\left[\frac{\omega}{0.6\pi}\right]^{2}}. \quad (5)$$

The following form has been chosen for the diminution factor $D(\omega)$:

$$D(\omega) = \exp[-ar]P(\omega, \omega_m), \quad (6)$$

where $P(\omega, \omega_m)$ is a kind of high-cut filter of arbitrary shape given by

$$P(\omega, \omega_m) = [1 + (\omega/\omega_m)^n]^{-1/2}, \quad (7)$$

where n is the power of the filter. The high-cut filter P is needed to account for the general observation that acceleration spectra often show an abrupt depletion of high-frequency energy above some frequency ($\omega_m = 2\pi f_{max}$).

Instrumentation response $I(\omega)$ is the response of the recording system to ground motion. It is given by:

$$I(\omega) = \frac{V\omega^2}{(\omega^2 - \omega_r^2) - 2\eta\, i\omega\omega_r}, \quad (8)$$

where V is the static magnification, ω_r is $2\pi f$ where f is the natural frequency of seismograph and η is the fractional damping.

The values of f and η in the present case are 25 Hz and 0.70.

The shape of the spectrum of recorded ground motion is greatly influenced by the spectral content of the source time function, form of the rupture process (unilateral, bilateral or circular rupture), velocity of rupture propagation and finiteness of the seismic source. In the convolution model used by Boore[18], a point earthquake source was used and details of the rupture process were omitted. In the present work, the finiteness of the earthquake source has been considered. The spectrum of source time function $S(\omega)$ has been so defined that it includes the effect of finiteness of the source.

$S(\omega)$ is defined as

$$S_o(\omega) = (-i\omega/\tau_c)F(\omega)\frac{\sin X_c}{X_c}\exp\left[i\left(\frac{\omega r_o}{c} + X_c\right)\right], \quad (9)$$

where

$$X_c = \frac{\omega L}{2}\left(\frac{1}{v} - \frac{\cos\psi}{c}\right),$$

$F(\omega)$ is the spectrum of the source time function, v is the rupture velocity, L is the length of the fault rupture,

$$\tau_c = \frac{L}{c}\left(\frac{c}{v} - \cos\psi\right).$$

The above form of the source spectral function takes into account source finiteness, the travel time r_o/c from the radiating point to the source, and the fact that in the far-field displacement is proportional to the time derivative of the source time function $f(t)$.

The fault plane is divided into a number of elementary faults or sub-faults. The dimension of each sub-fault is so chosen that the observation point is effectively in the far-field, in order to use the above formulation that is valid only in the far-field. The observation point will be effectively in the far-field if, the distance between the nearest radiating point

on the fault and the observation point is several times the dimension of the sub-fault.

The theoretical basis of computing synthetic accelerograms has been discussed above. Next the computational procedure has been discussed and presented to generate synthetic accelerograms.

The Garhwal Himalaya falls in the main Himalayan Seismic Zone. This region forms part of the boundary between the colliding Indian and Eurasian plates. The region is characterized by three major northward-dipping thrust zones separated by geological/physiographic sub-provinces. The northernmost province is the Greater Himalaya, which has an average elevation of 5 km and is composed of crystalline metamorphic and igneous rocks brought up along the Main Central Thrust (MCT). The sedimentary rocks in the south, which are mostly of Palaeozoic age, define the Lesser Himalaya sub-province, which is delimited by the Main Boundary Thrust (MBT) to its south[18]. These slightly metamorphosed sediments are overlain, in places, by a thrust sheet of the crystalline rocks. South of the MBT lies Outer Himalaya or Sub-Himalaya region with average elevation of a few hundred metres. This zone consists of folded and faulted Siwalik mollase sediments of Miocene Age.

In a widely accepted tectonic model[19], a detachment of fault represents the top surface of the northward underthrusting Indian plate over which wedges of Himalayan rock units are thrusted southwards. The local seismic activity in this region is largely concentrated in a relatively narrow belt, close to and primarily south of the surface trace of the MCT. Most earthquakes are located between part of Lesser Himalaya and immediate south of Higher Himalaya, extending from Nepal through Kumaun and Garhwal and western Himachal Pradesh.

Two-layer P velocity model has been based on the results of micro earthquake investigations[20]. According to this model, the P-wave velocity in the top layer is 5.2 km/s and that in the second layer is 6.0 km/s. The top layer is 16 km thick. The fault plane lies entirely in the top layer. We have considered homogeneous half space with properties of top layer.

For the purpose of generating synthetic accelerograms, a source model has to be specified. This includes spatio-temporal parameters of earthquake focus, fault geometry (dip and strike of the fault), slip distribution over the fault plane and source time geometry. For the sake of simplicity, the source is supposed to be a rectangular fault buried in a half space.

In the present study a ramp function with rounded shoulders is chosen as the source time function. The formula for the same is given by[21]:

$$f(t) = \begin{cases} 0 & , \quad t \le 0 \\ (t/T_o)(1-\sin\omega_o t/\omega_o t) & , \quad 0 \le t \le T_o \\ 1 & , \quad t \ge T_o \end{cases} \qquad (10)$$

where T_o is the rise time and $\omega_o = 2\pi/T_o$. This function is continuous everywhere and is easily differentiable. The above form is chosen to model slip as a function of time at a point on the fault. The velocity pulse emanating from the source is considered as:

$$v(t) = (1/T_o)(1 - \cos\omega_o t),\ 0 \le t \le T_o, \qquad (11)$$

and thus acceleration pulse is

$$a(t) = (\omega_o/T_o)\sin\omega_o t,\ 0 \le t \le T_o. \qquad (12)$$

To properly model the ground acceleration at the recording site which is near the epicentre, the slip distribution over the fault plane should be specified. For the purpose of generating synthetic accelerograms, the whole fault has been considered to be made of a number of sub-faults, each of size 1 km × 1 km. In the present work the slip is assumed to be distributed randomly.

For the purpose of applying the proposed method for generating synthetic accelerograms, two earthquake events were selected which were recorded at a number of recording stations in Uttaranchal region. These earthquakes are the Uttarkashi earthquake of 20 October 1991 and the Chamoli earthquake of 29 March 1999. A short account of relevant features of these two earthquakes is given below.

The Uttarkashi earthquake occurred on 20 October 1991 at 02 : 53 h (IST) in the Uttarkashi region in the northwestern Himalayas. The centroid moment tensor focal mechanism solution by Harvard University (*PDE Monthly*, October 1991) has been chosen in this study as the initial model. The Chamoli earthquake occurred on 29 March 1999 at 03 : 55 h (IST) north of Chamoli in the Lesser Himalayas.

The focal mechanism solution is given in Table 1 for both the earthquakes. The fault plane chosen for modelling strong ground motion is the one having parameters corresponding to NP1 in Table 1. The hypocentral distance and other parameters for some of the recording stations are given in Tables 2 and 3 for both the earthquakes[22,23]. The locations and recording stations along with the main tectonic features of the region are shown in Figure 1.

The amount of dislocation was adjusted with estimates of the length and width of the causative fault in such a way that the correct value of seismic moment is obtained. Accordingly, the causative fault is taken to be 24 km long and 16 km wide. Similarly, the fault size for Chamoli earthquake has

Table 1. Focal mechanism of Uttarkashi and Chamoli earthquakes

Source	Focal mechanism	Seismic moment (M_o) (dyn-cm)
Uttarkashi earthquake		
CMT (Harvard)	NP1: strike 317°, dip 14°, slip 115° NP2: strike 112°, dip 78°, slip 84°	1.8×10^{26}
Chamoli earthquake		
USGS	NP1: strike 282°, dip 9°, slip 95° NP2: strike 97°, dip 81°, slip 89°	1.8×10^{26}

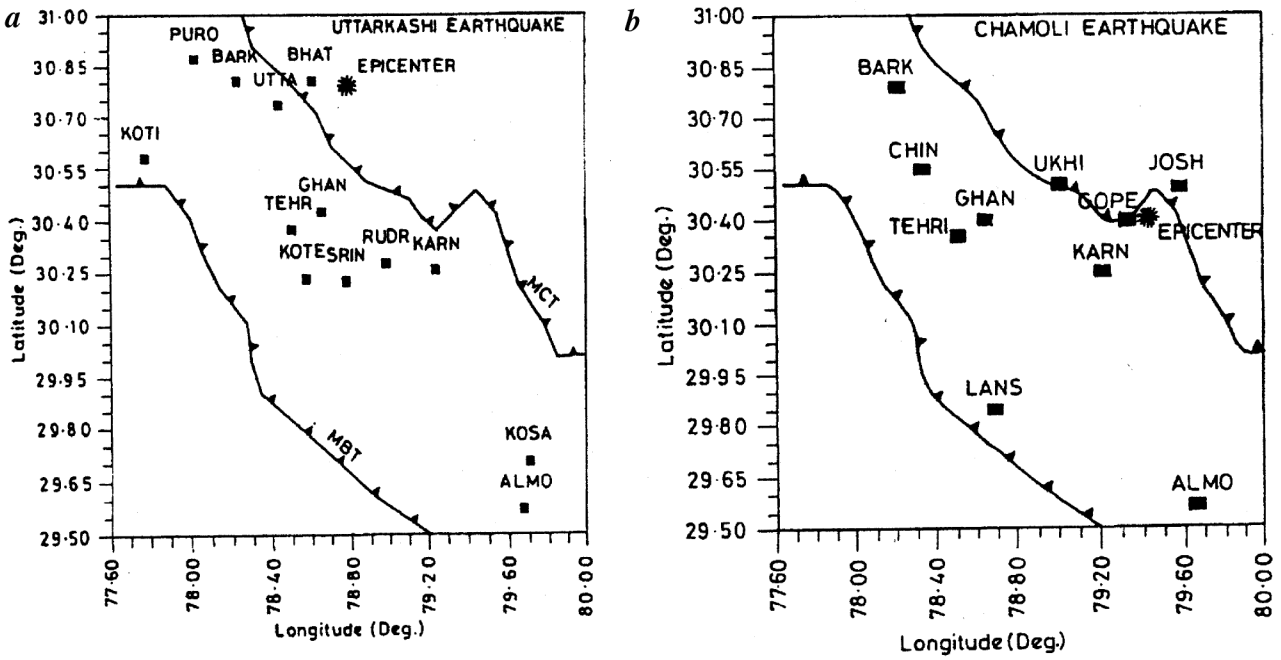

Figure 1. Location of the (*a*) Uttarkashi 1991 earthquake and (*b*) Chamoli 1999 earthquake and recording stations along with main tectonic features of the region.

Table 2. Details of selected stations for Uttarkashi earthquake

Station	Station coordinates	Epicentral distance (Δ) km	Components
Almora	29.58°N	162.30	L N53W
	79.65°E		T N37E
Barkot	30.80°N	61.55	L N10E
	78.22°E		T N80W
Bhatwari	30.80°N	19.40	L N85E
	78.60°E		T N05W
Karnaprayag	30.25°N	77.75	L N05W
	79.23°E		T N85E
Koteshwar	30.23°N	65.03	L N30W
	78.57°E		T N60E
Purolia	30.87°N	77.78	L N65W
	78.08°E		T N25E
Tehri	30.36°N	55.61	L N63W
	78.50°E		T N27E
Uttarkashi	30.73°N	36.41	L N15W
	78.45°E		T N75E

L, Longitudinal; T, Transverse.

Table 3. Details of selected stations for Chamoli earthquake

Station	Station coordinates	Epicentral distance (Δ) km	Components
Almora	29.58°N	94.44	L N53W
	79.65°E		T N37E
Barkot	30.80°N	141.58	L N10E
	78.22°E		T N80W
Gopeshwar	30.25°N	27.92	L N70W
	79.23°E		T N20E
Ukhimath	30.50°N	46.76	L N15E
	79.01°E		T N75W
Tehri	30.36°N	102.65	L N63W
	78.50°E		T N27E

Table 4. Source parameters for Uttarkashi and Chamoli earthquakes

Parameter	Earthquake	
	Uttarkashi	Chamoli
Length of fault (km)	24	36
Width of fault (km)	16	20
Focal depth (km)	10	15
Dip of fault (°)	14	8
Strike of fault (°N)	317	274
Rise time (s)	0.25	0.25
Rupture velocity (km/s)	2.30	2.50
Slip angle (°)	115	100
Rupture model	Circular rupture	Circular rupture
Source time function	Modulated ramp	Modulated ramp
Average slip (cm)	80	75
Maximum slip (cm)	170	160

been taken as 36 km long and 20 km wide. Source parameters for both the earthquakes are given in Table 4.

To generate the synthetic accelerograms, several numerical experiments were conducted to arrive at the optimum values of some key parameters which greatly affect the arrival times and phases of the recorded pulses. These source parameters are rise time (T_o), rupture velocity (v), slip angle (λ) and focal depth (h). Three rupture models were used, namely unilateral, bilateral and circular rupture. It was found that circular rupture gives the most satisfactory results.

As discussed earlier, a rectangular fault has been taken and divided into a number of sub-faults. To determine the duration of strong ground motion at the recording site, *P* and *S*-wave travel times were computed from each of the four corners of the fault. The largest *S*-wave travel time and

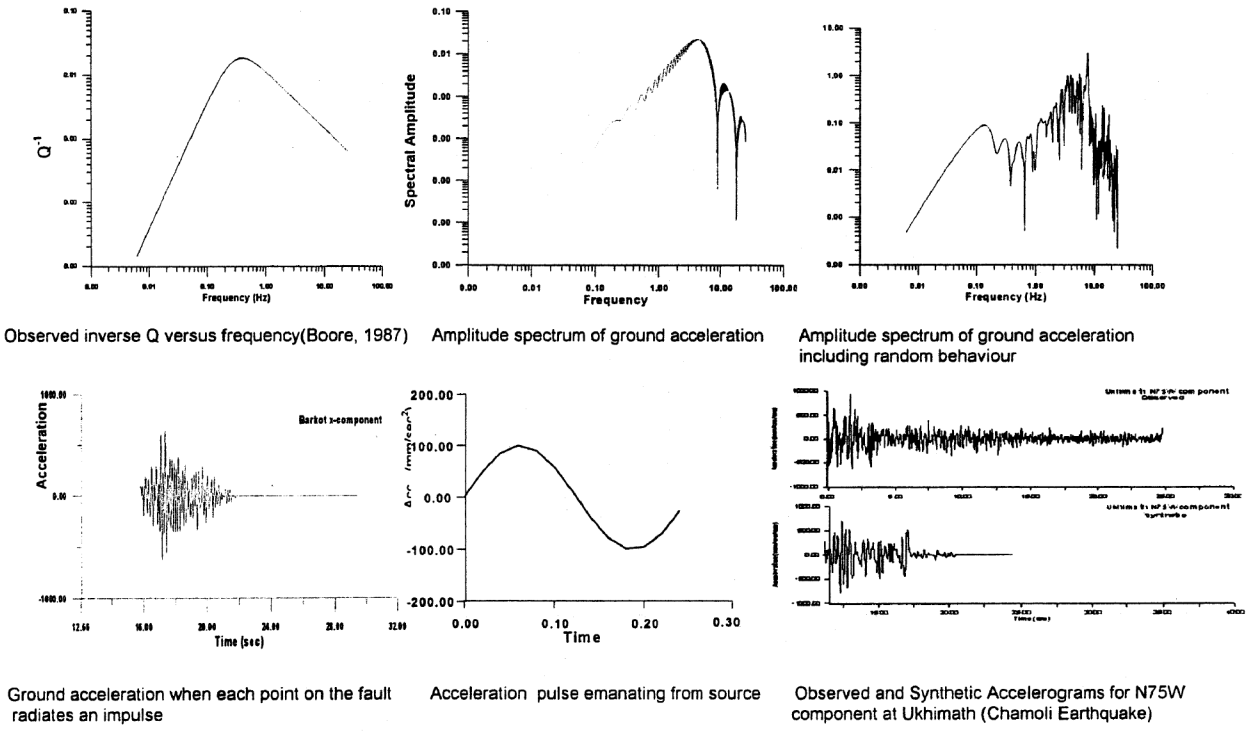

Figure 2. Schematic illustration of various steps for synthesizing accelerograms using the proposed method.

the smallest *P*-wave travel time were selected. The travel time of the *P*-wave directly from the focus was also computed, which is the smallest. If the smallest *P*-wave travel time from any of the corners of the fault happened to be smaller than that directly from the focus, then that time was taken as the smallest *P*-wave travel time.

Amplitude spectrum of ground acceleration is then calculated by summing the contribution from each sub-fault. It takes into account slip distribution (assumed random) on the fault plane, slip angle (assumed constant all over the fault), finiteness of the source, diminution factor and instrument response. This spectrum is then multiplied by the spectrum of Gaussian white noise to give the spectrum. This is inverse Fourier transformed to yield the time history. It represents the synthetic accelerogram as if each point on the fault had radiated an impulse. Convoluting this with source time function (the acceleration pulse) yields the final synthetic accelerogram shown in Figure 2. This procedure is repeated for every site where synthetic accelerograms have been generated.

The accelerographs which recorded the two Himalayan earthquakes were analogue recording devices. The strong ground motion data were recorded when these instruments were triggered by a strong pulse. In the case of these two earthquakes the instruments were not seen to have been triggered by the first *P*-wave. The later arriving *S*-waves are clearly seen on most records. It may have been due to the fact that the first *P*-wave was quite weak or the trigger level of the instrument was somewhat higher. As a result, the starting pulse on the observed accelerograms cannot be taken to be the first *P*-arrival. Consequently, the interval between arrival times of *S*- and *P*-waves on a synthetic accelerogram is of longer duration than that on corresponding observed accelerogram where initial pulse may be at a later phase after *P*-wave.

Figures 3 and 4 show the synthetic and observed accelerograms for Uttarkashi 1991 and Chamoli 1999 earthquakes for observed and synthetic accelerograms for longitudinal and transverse horizontal components. It is clear that the motion on synthetic accelerograms begins earlier than that on the observed ones. Both the synthetic and observed accelerograms are plotted on the same timescale. The match between the two sets of accelerograms is quite satisfactory in a number of cases. The differences in the two sets of accelerograms can be ascribed to the following causes:

(i) The effect of amplification of ground motion by near-surface unconsolidated materials has not been taken into account. The earth model chosen for the present study is that of a homogeneous half space. In real earth there are a number of inhomogeneities which lead to scattering of high frequency energy. Such scattering effects have been ignored.

(ii) The tail of the accelerogram consists of surface waves and backscattered waves. Such effects have not been taken into account.

(iii) In the Himalayan region, effects of topography in the vicinity of the recording station are likely to be important

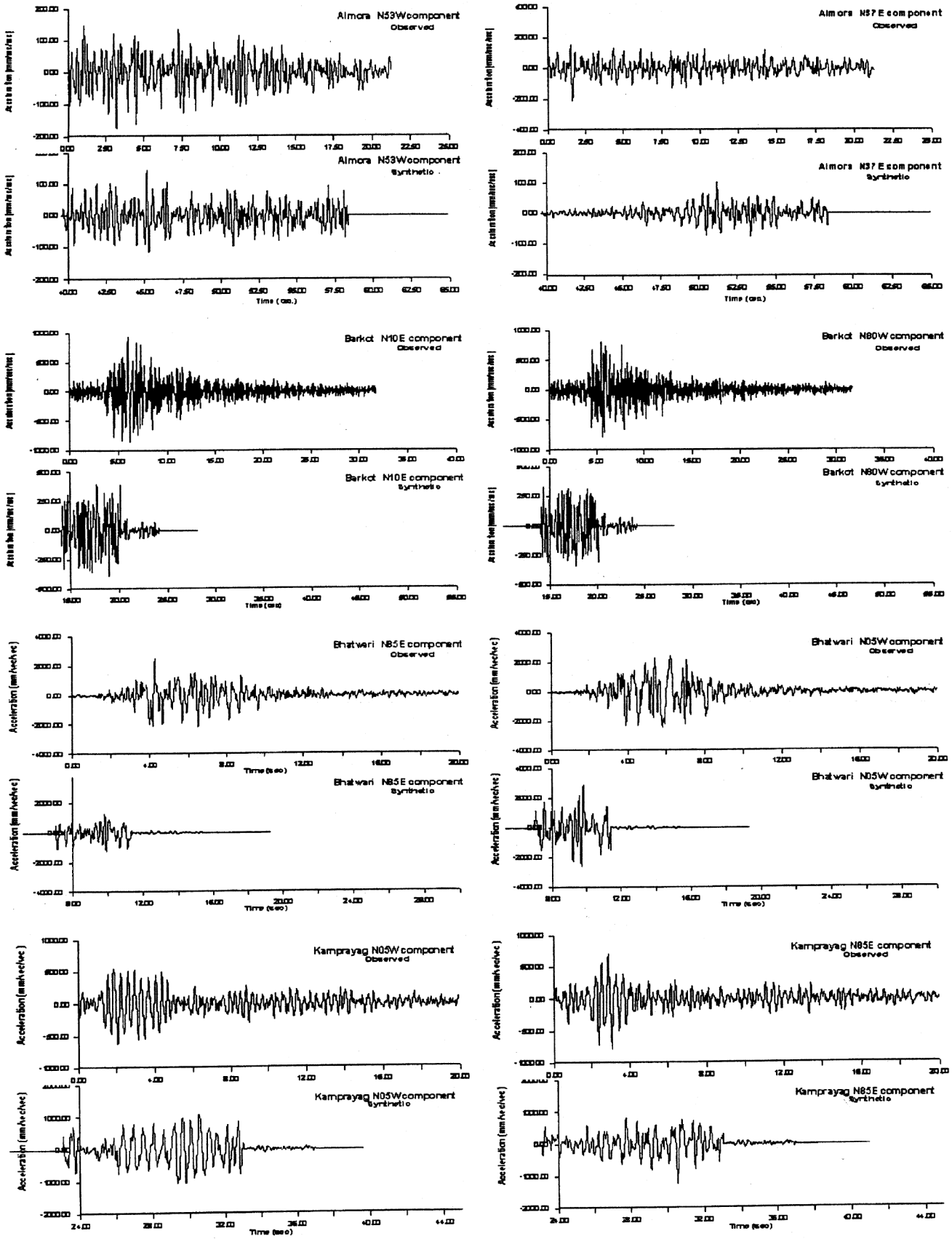

Figure 3. (*Continued*)

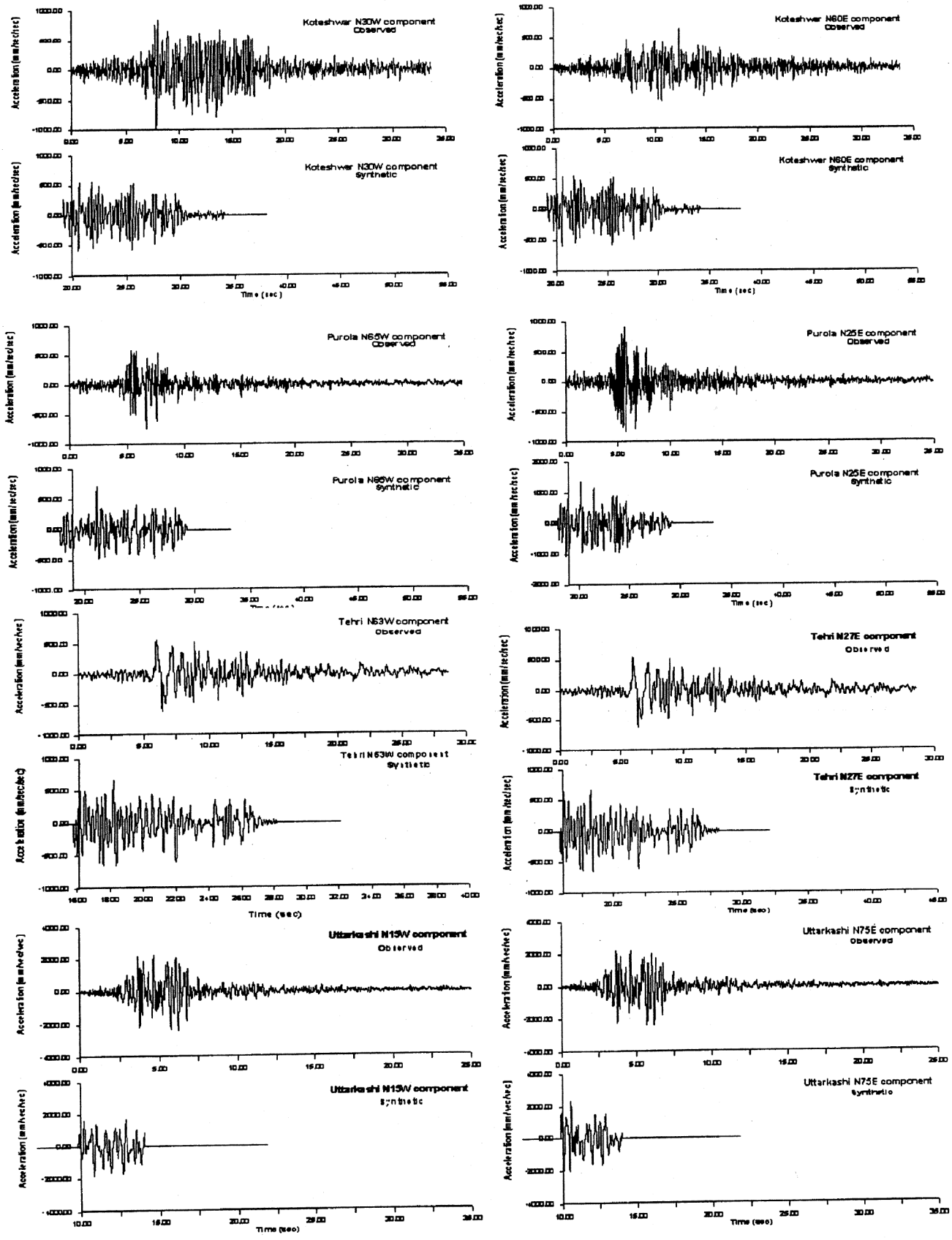

Figure 3. Comparison of observed (transverse and longitudinal components) accelerograms with synthetic accelerograms for Uttarkashi earthquake.

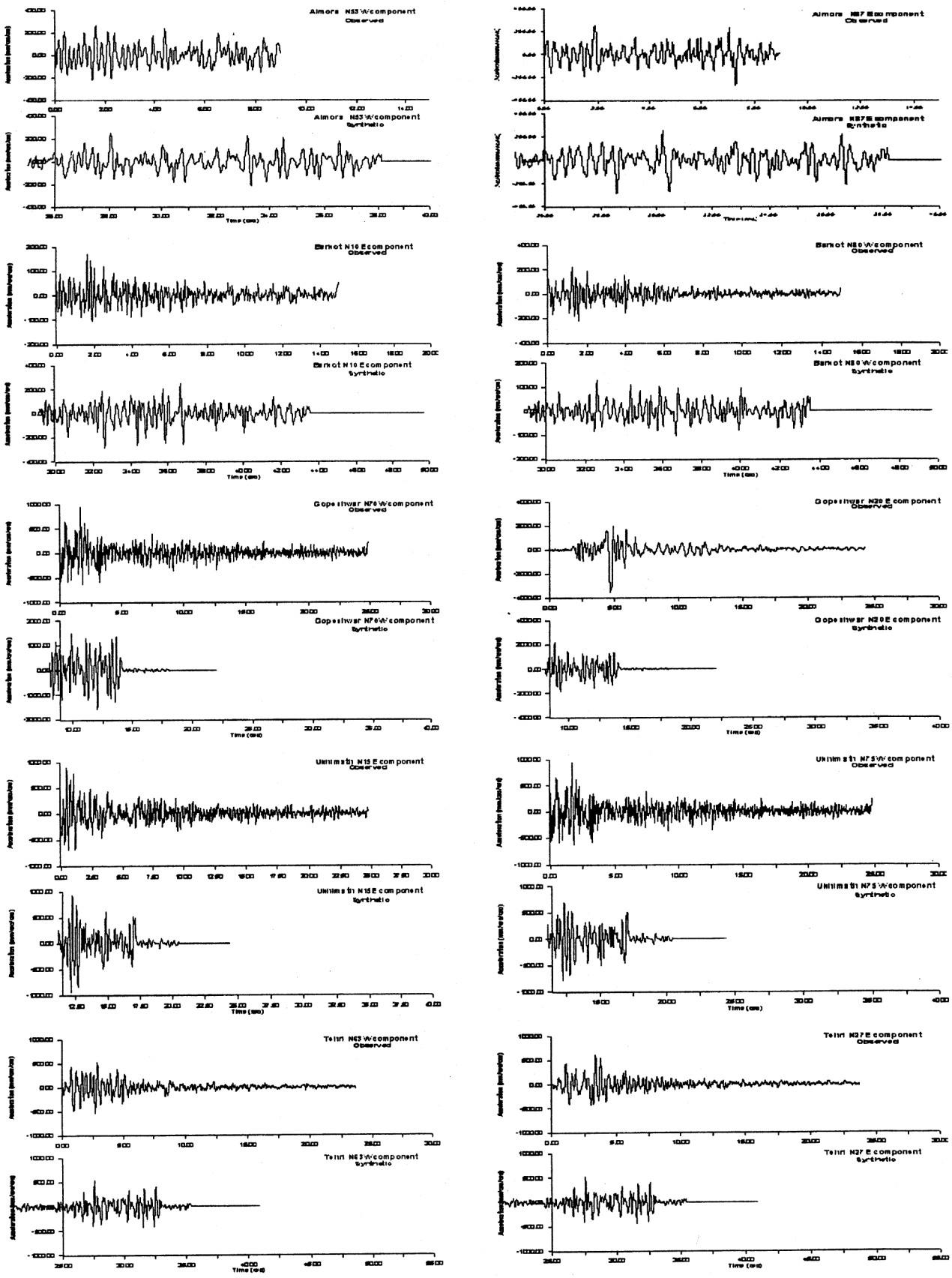

Figure 4. Comparison of observed (transverse and longitudinal components) accelerograms with synthetic accelerograms for Chamoli earthquake.

for the recorded ground motion. The record of ground motion from a recording station located on the side or bottom of a valley will be influenced by the shape of the valley. These effects have not been considered in the present study.

(iv) The recorded accelerogram is influenced by closeness of the causative fault, its size, pattern of slip distribution, form of source time function, rise time, rupture velocity and model of rupture propagation (unilateral, bilateral, circular, etc.). The size of the fault can be estimated. However, other properties of the source are not known in advance.

(v) As stated earlier the objective of the present study is to determine the usefulness of a method of synthetic seismogram generation proposed herein. The synthetic accelerograms generated in the present study show a satisfactory match with the observed ones in a number of sites, demonstrating the usefulness of the method of synthetic seismogram generation.

1. Abrahamson, N. P., Somerville, P. G. and Cornell, C. A., Goodness of fit for numerical strong motion simulations and uncertainty in numerical strong motion simulations predictions. Proceedings of the 4th US National Conference on Earthquake Engineering, Palm Springs, California, 1990, vol. 1, pp. 317–326.
2. Makaris, D. I., Stavrakakis, G. N. and Drakopoulos, J. C., Expected ground motion at a site based on hypothetical fault models. *Earthquake Engineering*, Tenth World Conference, Balkema, Rotterdam, 1992, vol. 2, pp. 703–708.
3. Barker, J. S., Somerville, P. G. and McLaren, J. P., Modelling of ground motion attenuation in Eastern North America. Electric Power Research Institute Report NP-5577, 1988, p. 414.
4. Wald, D. J., Helmberger, D. V. and Heaton, T. H., Rupture model of the 1989 Loma Prieta earthquake from the inversion of strong motion and broadband and teleseismic data. *Bull. Seismol. Soc. Am.*, 1991, **81**, 1540–1572.
5. Zeng, Y., Aki, K. and Teng, L., Source inversion of the 1987 Whittier narrows earthquake, California, using the isochron method. *Bull. Seismol. Soc. Am.*, 1993, **83**, 358–377.
6. Zeng, Y., Aki, K. and Teng, L., Mapping of the high frequency source radiation for the Loma Prieta earthquake, California. *J. Geophys. Res.*, 1993, **98**, 11981–11993.
7. Somerville, P., Engineering applications of strong ground motion simulation. *Tectonophysics*, 1993, **218**, 195–219.
8. Zeng, Y., Anderson, J. G. and Yu, G., A composite source model for computing realistic synthetic strong motions. *Geophys. Res. Lett.*, 1994, **21**, 725–728.
9. Zeng, Y., Anderson, J. G. and Su, F., Source and path effects in realistic strong ground motion simulation. *Seism. Res. Lett.*, Abstract, 1994, **65**, 36.
10. Khattri, K. N., Yu, G., Anderson, J. G., Brune, J. N. and Zeng, Y., Seismic hazard estimation using modeling of earthquake strong ground motions: A brief analysis of 1991 Uttarkashi earthquake, Himalaya and prognostication for a great earthquake in the region. *Curr. Sci.*, 1994, **67**, 343–353.
11. Yu, G., Khattri, K. N., Anderson, J. G., Brune, J. N. and Zeng, Y., Strong ground motion from the Uttarkashi, Himalaya, India, earthquake: Comparison of observations with synthetics using the composite source model. *Bull. Seismol. Soc. Am.*, 1995, **85**, 31–50.
12. Kumar, D., Khattri, K. N., Teotia, S. S. and Rai, S. S., Modeling of accelerograms of two Himalayan earthquakes using a novel semi-empirical method and estimation of accelerograms for a Hypothetical great earthquake in the Himalaya. *Curr. Sci.*, 1999, **76**, 819–830.
13. Khattri, K. N., Zeng, Y., Anderson, J. G. and Brune, J., Inversion of strong motion waveforms for source slip function of 1991 Uttarkashi earthquake, Himalaya. *J. Himalayan Geol.*, 1994, **5**, 163–191.
14. Kasahara, K., *Earthquake Mechanics*, Cambridge University Press, 1981.
15. Aki, K. and Richards, P. G., *Quantitative Seismology: Theory and Methods*, W. H. Freeman and Company, San Francisco, 1980, vols 1 and 2.
16. Boore, D. M., The prediction of strong ground motion. In *Strong Ground Motion Seismology* (eds Erdik, M. and Toksoz, M. N.), NATO Advanced Studies Institute Series, D. Reidel Publishing Company, Dordrecht, 1987, pp. 109–141.
17. Boore, D. M., Stochastic simulation of high frequency ground motions based on seismological models of the radiated spectra. *Bull. Seismol. Soc. Am.*, 1983, **73**, 1865–1894.
18. Valdiya, K. S., Tectonics and evolution of the central sector of the Himalaya. *Philos. Trans. R. Soc. London*, 1988, **4326**, 151–175.
19. Seeber, L. and Armbruster, J. G., Great detachment earthquakes along the Himalayan arc and long term forecasting. In *Earthquake Prediction: An International Review*, Maurice Ewing Series, 4, American Geophysical Union, Washington DC, 1981, pp. 259–277.
20. Khattri, K. N., Local seismic investigation in the Garhwal-Kumaon Himalayas. *Mem. Geol. Soc. India*, 1992, **23**, 45–66.
21. Ben-Menahem, A. and Singh, S. J., *Seismic Waves and Sources*, Springer-Verlag, New York, 1981, p. 1108.
22. Chandrasekaran, A. R. and Das, J. D., Strong motion records from Uttarkashi earthquake. *Mem. Geol. Soc. India*, 1995, 133–147.
23. IMD, Chamoli earthquake of 29 March 1999 and its aftershocks. India Meteorological Department, Government of India, Seismology No. 2/2000, 2000, p. 70.

ACKNOWLEDGEMENT. We thank the Director, CBRI, Roorkee and Head, Department of Earth Sciences, IIT Roorkee for support.

Received 22 April 2004; revised accepted 16 December 2004

The tsunami of the great Sumatra earthquake of *M* 9.0 on 26 December 2004 – Impact on the east coast of India

R. K. Chadha[1,*], G. Latha[2], Harry Yeh[3], Curt Peterson[4] and Toshitama Katada[5]

[1]National Geophysical Research Institute, Hyderabad 500 007, India
[2]National Institute of Ocean Technology, Chennai 601 302, India
[3]Department of Civil Engineering, Oregon State University, Corvallis, Oregon 97336-4501, USA
[4]College of Liberal Arts and Science, Portland State University, Portland, Oregon 97207, USA
[5]Gunma University 1-5-1, Tenjincho, Kiryu, Gunma, 376-8515, Japan

An earthquake of magnitude 9.0 occurred off the coast of Sumatra on 26 December 2004 at 00 : 58 : 50 (UTC)/ 06 : 28 : 50 AM (IST). The epicentre of the earthquake was located at 3.29°N and 95.94°E. The focal depth of

*For correspondence. (e-mail: chadha@ngri.res.in)